A&A 408, 961–969 (2003)
DOI: 10.1051/0004-6361:20030939


Astronomy & Astrophysics

# 35 cm observations of a sample of large supernova remnants⋆

W. Reich[1], X. Zhang[1,2], and E. Fürst[1]

[1] Max-Planck-Institut für Radioastronomie, Auf dem Hügel 69, 53121 Bonn, Germany
[2] National Astronomical Observatories, CAS, Beijing 100012, China

Received 9 April 2003 / Accepted 16 June 2003

**Abstract.** We present radio maps of ten large-diameter supernova remnants observed at 35 cm wavelength with the Effelsberg 100-m telescope. The angular resolution is 14′.5. The sources are G126.2+1.6, G127.1+0.5, HB3, HB9, S147, IC 443, Cygnus Loop, W63 and HB21. For each object we give an integrated flux density and improved spectra when necessary. We also present a map of G213.0−0.6, which we tentatively identify as a new large supernova remnant with a very low surface brightness, apparently interacting with the H II region S284.

**Key words.** ISM: supernova remnants – radio continuum: ISM

## 1. Introduction

Shell-type supernova remnants (SNRs) emit synchrotron radiation with a non-thermal spectrum. The majority of known SNRs are in the adiabatic expansion phase with a radio spectrum close to $\alpha = 0.5$ ($S \sim \nu^{-\alpha}$). Such spectra are expected from electrons accelerated in a strong shock.

Most of the intense large-diameter SNRs have already been identified from the first radio surveys made at low frequencies (e.g. Brown & Hazard 1953; Westerhout 1958). Subsequent measurements were made mainly in the frequecy range below 1 GHz. These early data were limited in sensitivity due to the receiver equipment available. When made with small single-dish telescopes they have a coarse angular resolution which often barely resolves the SNRs. Accurate flux densities were not available for many sources. The use of synthesis telescopes with much higher angular resolution resulted in numerous very detailed maps of these SNRs and spectral studies of small-scale structures became possible. However, large-scale structures were not well measured, because of missing zero spacings. Therefore integrated flux densities from synthesis telescope data have to be taken as lower limits. Spectral changes or breaks at high frequencies are a clue to the physical conditions and the evolution of SNRs. Precise flux densities and spectra of SNRs over a wide frequency are required. Therefore we made observations at 35 cm wavelength with the Effelsberg 100-m telescope to measure accurate integrated flux densities. Detailed studies of some of the sources in comparison with radio maps at other frequencies are given elsewhere.

We describe the observations in Sect. 2, discuss each source in turn in Sect. 3 and make some concluding remarks in Sect. 4.

## 2. Observations and data reduction

The Effelsberg 100-m radiotelescope was used to observe a sample of large-diameter SNRs at 35 cm wavelength. A crossed dipole in the prime focus of the telescope served as the feed. It was followed by a hybrid converting the received signals into a left-hand and a right-hand circularly polarised component. Each component was amplified by an uncooled HEMT-receiver operating in total-power mode. The receiver can be used within a frequency range from 800 MHz to 1.3 GHz. Its main purpose is to search for highly redshifted H I emission. This frequency band is not protected for the requirements of radio astronomy and indeed many terrestrial signals of different origin mask any sky signal. Fortunately test measurements (Lochner & Fürst 1997) showed that a number of narrow sub-bands could be used at least occasionally for continuum observations. Nevertheless, it turns out that the wide frequency range of the first stage of the receiver is a problem for sensitive continuum observations, since strong interference causes saturation and narrow-band filtering in the IF-stage was therefore insufficient.

A significant improvement was obtained by adding a narrow HF-filter in front of the HEMT-receivers. This filter was centered at 863 MHz with a 3dB-width of 30 MHz. The installation of this filter makes sensitive observations possible, and the IF-bandwidth selected was between 2 MHz and 10 MHz within the 30 MHz-wide band. Slightly different centre frequencies were used. The fraction of time lost due to interference was reduced to about 10% to 20% of the allocated observing time.

*Send offprint requests to*: W. Reich,
e-mail: wreich@mpifr-bonn.mpg.de

⋆ Based on observations with the Effelsberg 100-m telescope operated by the Max-Planck-Institut für Radioastronomie (MPIfR), Bonn, Germany.

**Table 1.** Observational parameters.

| Source | Map size [°] | Coord. System | No. of coverages |
|---|---|---|---|
| G126.2+1.6/G127.1+0.5 | $4 \times 4$ | LB | 4 |
| G132.7+1.3(HB3) | $4 \times 4$ | LB | 9 |
| G160.9+2.6(HB9) | $4.2 \times 4.2$ | LB | 7 |
| G180.0−1.7(S147) | $5 \times 5$ | LB | 6 |
| G189.1+3.0(IC 443) | $4.8 \times 4$ | LB | 6 |
| G213.0−0.6 | $5 \times 5$ | LB | 4 |
| G74.0−8.5(Cygnus Loop) | $6.4 \times 5$ | $\alpha\delta$ | 4 |
| G82.2+5.3(W63) | $4.2 \times 4.2$ | LB | 5 |
| G89.0+4.7(HB21) | $4 \times 4$ | $\alpha\delta$ | 4 |

Successful observations were made during three nights in December 1999 and five nights in August 2000. Only nighttime data were used because of the telescope's far-sidelobe response to solar radiation. A number of relevant parameters of the receiving system are included in the test reports by Lochner & Fürst (1997, 1998). They measured an aperture efficiency of the telescope of about 45%, which indicates a low feed illumination of the telescope resulting in low sidelobe levels. The first sidelobes are at about 20 dB along the direction of the feed support legs and below elsewhere. We measured a HPBW of the Gaussian main beam of $14\farcm8 \times 14\farcm3$ in December 1999 and $14\farcm6 \times 14\farcm3$ in August 2000. This results in an intensity conversion $T_{\rm B}[{\rm K}]/S\,[{\rm Jy}] = 2.18 \pm 0.08$ for main-beam brightness temperatures and flux densities.

All SNRs were mapped several times. The telescope was moved alternately in two orthogonal directions. Details for all sources including their Galactic designation are listed in Table 1, where the number of coverages also includes incomplete maps or maps where sections were lost due to interference. The standard reduction procedures for Effelsberg continuum observations were used. Afterwards the individual maps have been edited for spiky interference, de-striped using the "unsharp masking method" (Sofue & Reich 1979) and finally combined with the "Plait" algorithm (Emerson & Gräve 1988). The final maps all have relative zerolevels with zero at their boundaries. Any offset or gradient of Galactic large scale emission is removed that way.

Flux densities for calibration sources were not directly available at 865 MHz. 3C 286 served as the main calibrator for which we assumed a flux density of 18.5 Jy. This agrees with the average of data interpolated from Baars et al. (1989) and Kühr et al. (1981) and extrapolated from Ott et al. (1994). 3C 48 and 3C 138 served as secondary calibrators, where we measured flux densities relative to 3C 286. They were used to calibrate all of our August 2000 measurements, because 3C 286 was not observable within the allocated observing time. We list the flux densities of the calibration sources in Table 2 and also give the catalogue values. We did not correct the scale for observations which were a few MHz off from 865 MHz. Differences are very small when compared to the accuracy of the absolute flux density scale.

**Table 2.** 865 MHz flux densities of calibration sources.

| Source | $S$ [Jy]* | Baars et al. | Kühr et al. | Ott et al. |
|---|---|---|---|---|
| 3C 286 | 18.5 | 18.5 | 18.8 | 17.9 |
| 3C 48 | 22.4 | 23.1 | 22.4 | 23.7 |
| 3C 138 | 11.2 | – | 12.3 | – |

* Adopted flux density.

## 3. Results

We list the derived integrated flux densities for the observed SNRs in Table 3. The measured noise for each of the maps as shown below is also included. The confusion limit at the Effelsberg telescope is calculated to be about 25 mJy/b.a. when extrapolated from higher frequency data, and some noise values come close to that limit. Low-level interference and mainly fluctuating background emission raise the noise limit slightly. The northern sky survey of Berkhuijsen (1972) at 820 MHz is close to the present observing frequency and shows the level of Galactic emission for the fields observed. For the flux integrations we assume a constant background across the SNRs. Table 3 lists the local mean background level adopted and also the size of the SNRs as measured from the present maps.

Two general compilations of fitted SNR spectra are available from Trushkin (2002) and from Kovalenko et al. (1994a,b), which are based on literaure values and on their own measurements. We compare our results with these spectra in cases where no detailed investigations of the individual SNRs are available.

### 3.1. G126.2+1.6 and G127.1+0.5

The two shell-type SNRs have been previously observed in the radio range, where the most recent studies are by Joncas et al. (1989) and by Fürst et al. (1984) presenting maps at arcmin angular resolution in the range from 408 MHz to 4.75 GHz. The Effelsberg map of the two SNRs at 865 MHz is shown in Fig. 1.

At $14\farcm5$ angular resolution the remarkable central source in G127.1+0.5 is barely resolved. It is a variable flat-spectrum source with a spectral low-frequency turnover at about 2 GHz. Despite the location of the source exactly at the geometrical centre of G127.1+0.5 it is believed to be of extragalactic origin based on its redshift ($z = 0.018$, Spinrad et al. 1979), although it has a number of similarities to SS433 which is located in the centre of the SNR W50 (e.g. Geldzahler & Shaffer 1981, 1982). We estimate the flux density of the central source to be about 0.3 Jy, in agreement with the spectrum shown by Joncas et al. (1989). Both SNRs are surrounded by diffuse emission including extended thermal emission at $l, b \sim 127\fdg9,\ 1\fdg9$ (Fürst et al. 1984) suggesting both sources to be located in the same area of the Galaxy. However, the absolute distance of both sources is quite uncertain. From the discussion by Joncas et al. (1989) a lower limit of 2 kpc and an upper limit of 5 kpc seems most likely.

**Table 3.** Integrated flux densities.

| Source | $S$ [Jy] | BG [Jy] | RMS [mJy] | Size [′ × ′] | PA [°]$^+$ |
|---|---|---|---|---|---|
| G126.2+1.6 | $6.1 \pm 1.6^*$ | 0.19 | 30 | 70 × 70 | |
| G127.1+0.5 | $14.6 \pm 0.8^*$ | 0.26 | 30 | 60 × 60 | |
| G132.7+1.3 (HB3) | $51.5 \pm 3.5$ | 0.49 | 27 | 130 × 95 | −20° |
| G160.9+2.6 (HB9) | $91 \pm 3$ | 0.11 | 30 | 135 × 135 | |
| G180.0−1.7 (S147) | $77 \pm 10^*$ | 0.10 | 35 | 200 × 180 | 90° |
| G189.1+3.0 (IC 443) | $160 \pm 5$ | 0.50 | 35 | 70 × 65 | 0° |
| G213.0−0.6 | $22.0 \pm 3.7^*$ | 0.05 | 28 | 160 × 140 | 105° |
| G74.0−8.5 (Cygnus Loop) | $184 \pm 18$ | 0.03 | 30 | 240 × 170 | 0° |
| G82.5+5.3 (W63) | $82.5 \pm 5.5$ | 1.50 | 40 | 100 × 70 | 60° |
| G89.0+4.7 (HB21) | $228 \pm 5$ | 0.26 | 40 | 120 × 105 | 90° |

BG is the mean local background level in the map subtracted for flux integration.
$^*$ Point sources subtracted; + counterclockwise direction.

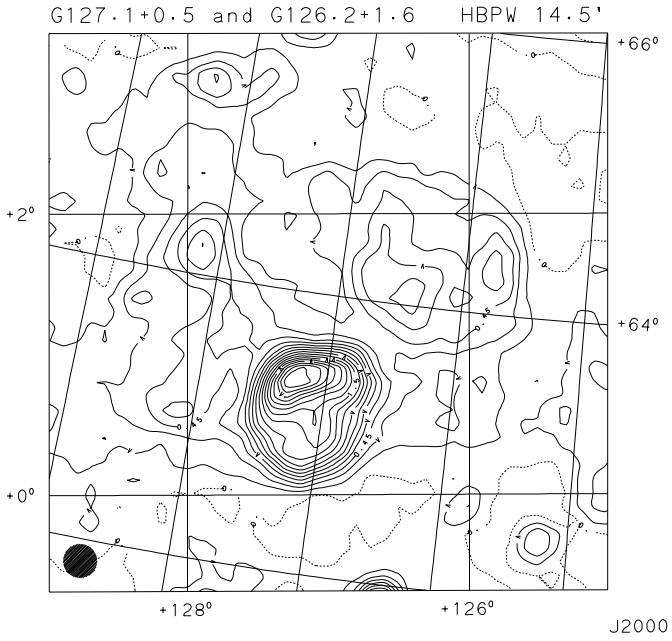


**Fig. 1.** Total intensities of G126.2+1.6 and G127.1+0.5 and the surrounding emission area at 865 MHz. Contours run in steps of 150 mJy/b.a.

We derive an integrated flux density of G126.2+1.6 of 7.1 ± 1.6 Jy and for G127.1+0.5 of 14.9 ± 0.8 Jy including the contribution of unresolved extragalactic sources in the field. Correcting for the contribution of sources by using the 408 MHz data of Joncas et al. (1989) scaled with a spectral index of $\alpha = 0.8$, yields flux densities for G126.2+1.7 and G127.1+0.5 of 6.1 ± 1.6 Jy and 14.6 ± 0.8 Jy, respectively.

The spectrum for G127.1+0.5 was fitted by Fürst et al. (1984) for the frequency range between 178 MHz and 4.85 GHz by a value of $\alpha = 0.6$, where their measured 4.85 GHz flux density exceeds that from the fitted spectrum. From his compilation of flux densities ranging from 38 MHz to 4.85 GHz Trushkin (2002) fitted a spectral index of $\alpha = 0.61$ at 400 MHz and $\alpha = 0.63$ at 4 GHz, close to the value of Fürst et al. (1984). Also Kovalenko et al. (1994b) report $\alpha = 0.59 \pm 0.17$. Our flux density at 865 MHz supports a spectrum for G127.1+0.5 of about $\alpha = 0.6$.

The spectrum of G126.2+1.6 was fitted by Fürst et al. (1984) with a spectral index of $\alpha = 0.48$ from Effelsberg flux densities at 1410 MHz and 2695 MHz. The spectrum might steepen towards higher frequencies. Our 865 MHz flux density agrees with the $\alpha = 0.48$ spectrum. Joncas et al. (1989) fitted $\alpha = 0.58$ when they include their 408 MHz flux density of 12.0 ± 2.5 Jy. Also Kovalenko et al. (1994b) fitted $\alpha = 0.59 \pm 0.12$. Trushkin (2002) fitted an even steeper spectrum with $\alpha = 0.77$ including RATAN–600 data at 960 MHz, 3650 MHz and 3900 MHz and in particular the high 83 MHz flux density of 35 ± 7 Jy from Kovalenko et al. (1994b). More precise low-frequency flux densities are needed for G126.2+1.6.

### 3.2. G132.7+1.3 (HB3)

The shell of the SNR HB3 is located at the western edge of the H II region complex W3-W4-W5 at a distance of about 2.2 kpc. HB3 is a rather evolved SNR with well correlated radio and optical filaments (Fesen et al. 1995).

We show the 865 MHz contour map in Fig. 2. At 14′.5 of angular resolution W3 ($l = 133.7°, b = 1.2°$) is a barely resolved strong source (HPW = 22′.3 × 17′.6) with a peak flux density of about 51.8 Jy and an integrated flux density of about 95 Jy. A part of the extended W4 complex is seen towards the south-east of W3. It is evident from the complex surrounding of HB3 that an accurate integrated flux density is difficult to obtain. This limitation holds not only for the present observations, but also for most of the previously published maps with larger beam sizes. Subtracting W3 we get an integrated flux density for HB3 of about 51.5 ± 3.5 Jy in reasonable agreement with an extrapolated flux density of 47.8 Jy from the $\alpha = 0.6 \pm 0.04$ spectrum derived by Landecker et al. (1987).

Trushkin (2002) calculated a flatter spectrum with $\alpha = 0.49$ when adding RATAN–600 data at 3.65 GHz and 3.90 GHz, which predicts about 57.8 Jy at 865 MHz. Kovalenko et al. (1994b) report $\alpha = 0.51 \pm 0.12$ and their spectrum predicts about 60.5 Jy.

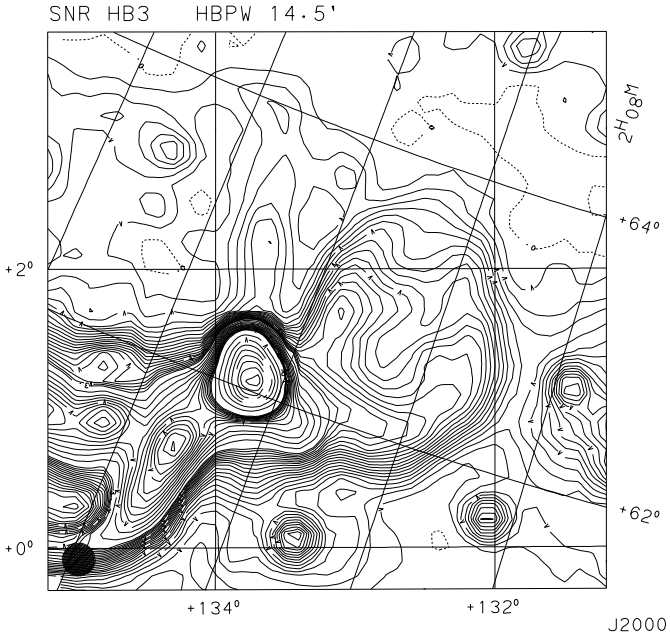


**Fig. 2.** Contour plot of G132.7+1.3 (HB3) and the surrounding area including the bright H II region W3 at 865 MHz. Contours run in steps of 150 mJy/b.a. up to 3 Jy/b.a., in steps of 500 mJy/b.a. up to 10 Jy/b.a. and in steps of 5 Jy/b.a. above.

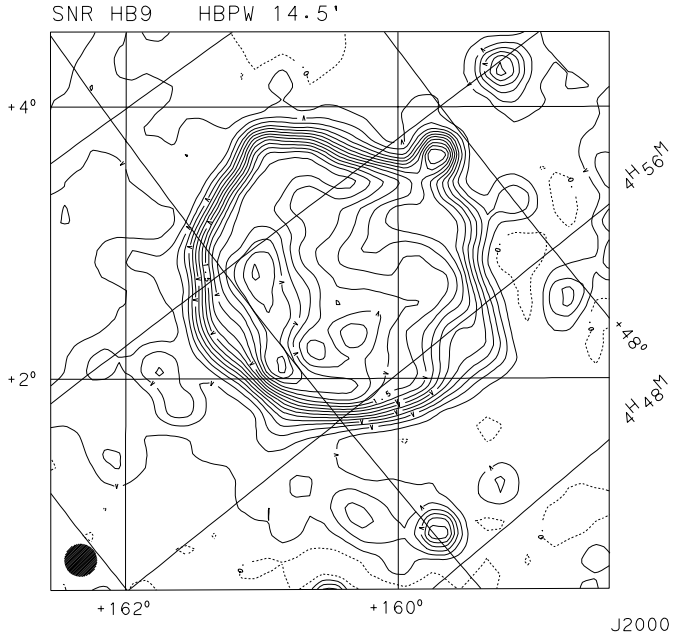


**Fig. 3.** Contour plot of HB9 as observed at 865 MHz. Contours run in steps of 150 mJy/b.a. up to 1.5 Jy/b.a. and in steps of 300 mJy/b.a. above.

### 3.3. G160.9+2.6 (HB9)

Observations of HB9 were previously made between 10 MHz and 5 GHz. Trushkin (2002) calculated a spectral index of $\alpha = 0.54$ for frequencies above 30 MHz. For lower frequencies some flattening of the spectrum most likely due to thermal absorption is observed. A number of reported flux densities deviate significantly from the spectral fit. We show the contour map of HB9 at 865 MHz in Fig. 3. Our 865 MHz flux density of 91 Jy is clearly below the expectation of about 125 Jy from Trushkin's spectrum. We have used an unpublished Effelsberg 4.75 GHz map, which was already included in the spectral index study by Leahy et al. (1998), to find the spectral index of HB9. We have made a temperature-versus-temperature plot (TT-plot, Fig. 4) of the two maps at the same angular resolution and grid. The slope of the plot gives the spectral index, which is largely independent of temperature offsets of the individual maps. The result of a linear fit of the TT-plot of HB9 was $\alpha = 0.57 \pm 0.03$, which is rather close to Trushkin's value. The discrepancy in the integrated flux densities is likely due to the presence of an emission plateau, which is clearly visible towards the south-east of HB9 (Fig. 3) and might be included in flux integrations of lower angular resolution maps. Alternatively Kovalenko et al. (1994b) fitted available flux density data with a spectral index $\alpha = 0.48 \pm 0.2$ below about 1.5 GHz and $\alpha = 0.96 \pm 0.5$ above. We do not think the evidence for a spectral break is convincing.

### 3.4. G180.0–1.7 (S147)

S147 is one of the most evolved SNRs and is located in the direction of the Galactic anticentre. It has been observed at radio

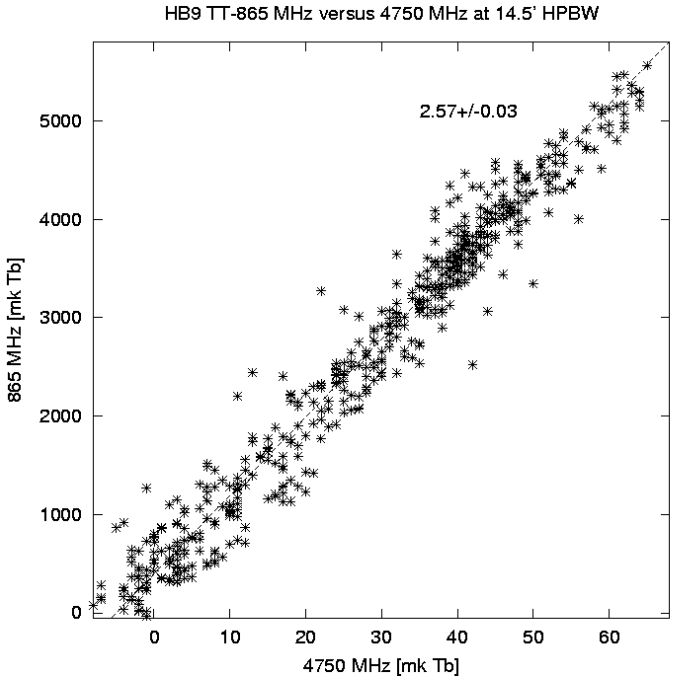


**Fig. 4.** Temperature-versus-temperature plot of HB9 observed at 865 MHz and 4750 MHz. The fit gives a temperature spectral index of $2.57 \pm 0.03$ corresponding to $\alpha = 0.57 \pm 0.03$.

frequencies between 81.5 MHz and 4995 MHz (see Fürst & Reich 1986; Trushkin 2002). S147 is supposed to be one of the rare SNRs showing a spectral break or bend of its integrated spectrum towards high frequencies. The determination of the break frequency is limited by the insufficient accuracy of the radio flux density values below 1 GHz, especially at 960 MHz (Harris 1962). The new measurements should define the radio spectrum below 1 GHz more precisely.

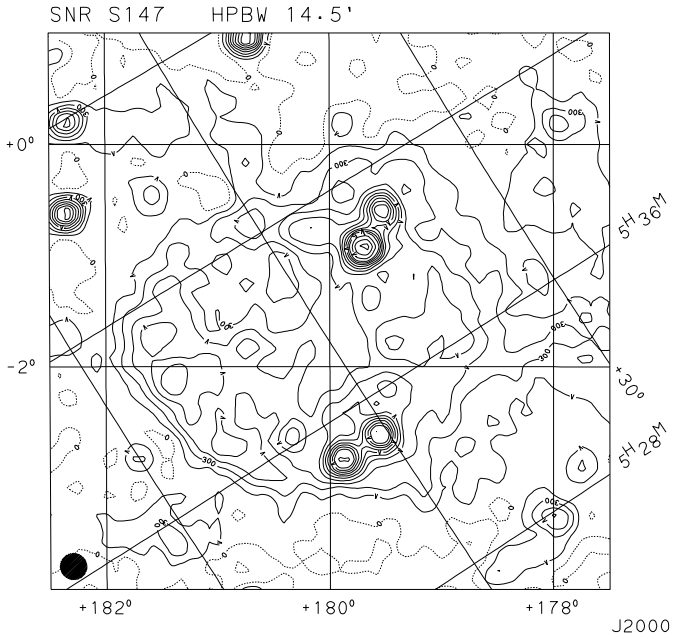


**Fig. 5.** Contour plot of S147 at 863 MHz. Contours are plotted from 0 to 0.6 Jy/b.a. in steps of 0.1 Jy/b.a., up to 1.0 Jy/b.a. in steps of 0.2 Jy/b.a., and further in steps of 0.25 Jy/b.a.

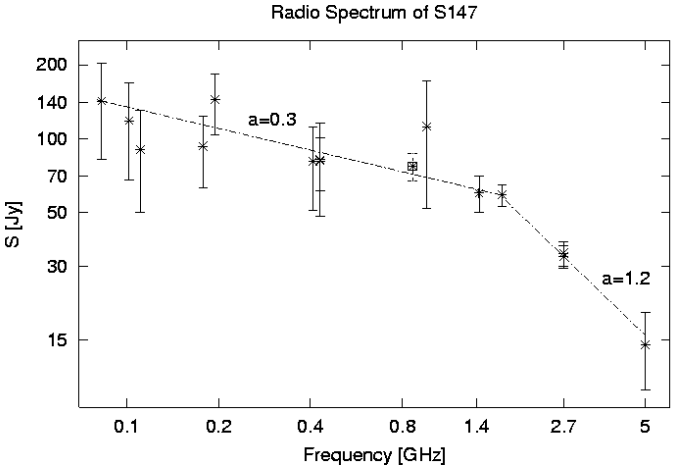


**Fig. 6.** Radio spectrum of S147. Flux densities for S147 from the literature were corrected by subtracting the flux density of compact sources listed by Fürst et al. (1982). Omitting the quite uncertain 960 MHz flux density the low-frequency spectrum of S147 has a spectral index $\alpha \sim 0.3$. Above the spectral break the spectral index is $\alpha \sim 1.2$.

The new map at 863 MHz is shown in Fig. 5. The shell structure is clearly defined. Four strong compact sources are visible within the boundary of the SNR. These sources have been observed by Angerhofer & Kundu (1981), Fürst et al. (1982) and Kim (1988). They are identified as extragalactic background sources. The angular resolution at 863 MHz is too low to identify the other background sources listed by Fürst et al. (1982). To compare the new measurement with the radio spectrum published by Fürst & Reich (1986) the integrated flux density of S147 at 863 MHz has been calculated after subtracting the extrapolated flux density of all listed background sources. The result is $77 \pm 10$ Jy. The radio spectrum is shown in Fig. 6. The low-frequency radio spectrum up to about 1.4 GHz is now represented by a spectral index of about $\alpha \sim 0.3$. The spectral break occurs between 1.5 GHz and 2 GHz. It was shown by Fürst & Reich (1986) that the spectral break results from the diffuse emission component of S147, while the filaments keep the flat spectrum towards higher frequencies. This indicates that S147 is a rather evolved SNR, where cosmic-ray electrons radiate in a compressed magnetic field. The higher magnetic field within the filaments shifts the spectral break of the cosmic-ray electron spectrum towards higher frequencies.

The 143 ms pulsar PSRJ0538+2817 (Anderson et al. 1996) is located within S147 and believed to be associated as the distance estimates for both the SNR (0.8–1.6 kpc) and the pulsar (1.2 kpc) agree. The characteristic age of the pulsar of $6 \times 10^5$ yr is much larger than the estimated $10^5$ yr based on radio data (Sofue et al. 1980). To account for this difference Romani & Ng (2003) propose an initial birth spin period of ≥130 ms. However, the age estimate of the SNR is based on its expansion into the average interstellar medium, which in the presence of a massive progenitor star will be modified by its stellar wind. In that case the expansion in a cavity is quite fast and quickly slowed down at the cavity walls.

### 3.5. G189.1+3.0 (IC 443)

The bright SNR IC 443 has been the subject of numerous investigations across the entire spectrum. IC 443 is in physical interaction with the H II region S249 located north of IC 443. Shocked molecular gas has been detected in the interacting region (Wang & Scoville 1992). IC 443 consists of three subshells, which are visible at high angular resolution in the radio and the infrared (Braun & Strom 1986). IC 443 is also bright in X-rays and associated to the $\gamma$-ray source 2EG J0618+2234 (Sturner & Dermer 1995; Esposito et al. 1996). Olbert et al. (2001) reported on a bow shock nebula associated with IC 443, which is most likely powered by a young neutron star. Based on ROSAT X-ray data Asaoka & Aschenbach (1994) identified a second SNR G189.6+3.3 located in front of IC 443 and believed to be an old evolved object.

Previous radio studies were made with single-dish telescopes and also with interferometers. Low angular resolution maps suffer from confusion of IC 443 with S249, while interferometric observations are insensitive to large scale structures. Figure 7 shows the 868 MHz map, which reveals extended structure surrounding both IC 443 and S249. Weak ridges extending east and north-east of IC 443 at $b \sim 2.^\circ5$ and $b \sim 3.^\circ5$ might belong to the SNR G189.6+3.3. The radio spectrum of IC 443 is reasonably well fitted by a power-law spectrum from about 30 MHz to 10 GHz, despite some spectral index variations across the SNR (Green 1986). Below 30 MHz some thermal absorption is present. Trushkin's fit (2002) of available flux densities gives $\alpha = 0.38$ and our integrated flux density of $160 \pm 5$ Jy is slightly below his fitted spectrum, which predicts 168 Jy. Kovalenko et al. (1994b) fitted $\alpha = 0.42 \pm 0.08$ and predict 174 Jy at 868 MHz.

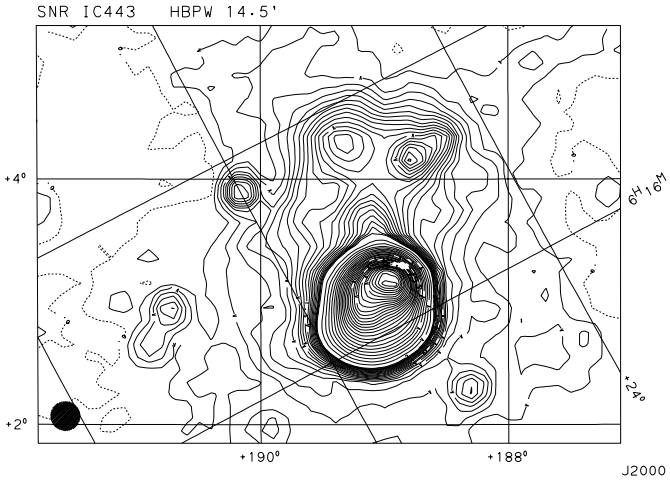


**Fig. 7.** Contour plot of IC 443 as observed at 868 MHz. Contours run in steps of 150 mJy/b.a. up to 1.5 Jy/b.a.

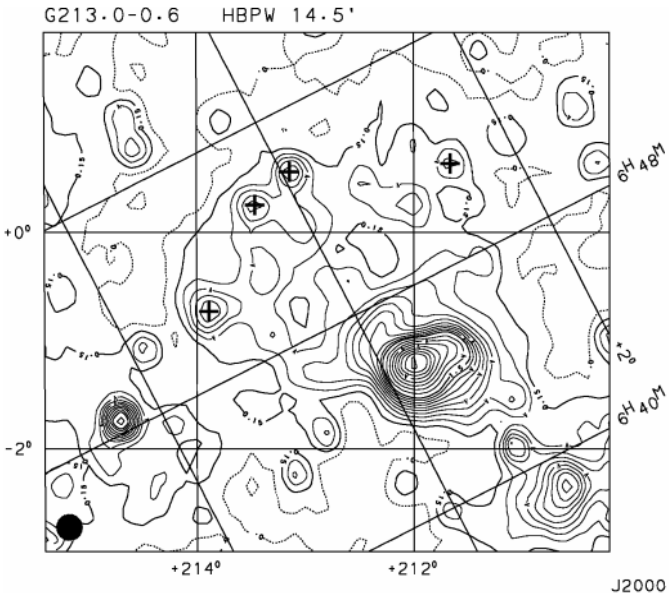


**Fig. 8.** Contour plot of G213.0−0.6 as observed at 863 MHz. Contours run in steps of 150 mJy/b.a. up to 1.5 Jy/b.a. and further in steps of 300 mJy/b.a. Four discrete sources as marked in the figure were subtracted before flux integration. Their integrated flux density is 3.25 Jy.

### 3.6. G213.0−0.6

The field shown in Fig. 8 in the Galactic anticentre direction was observed to clarify the nature of a faint emission plateau extending north-east of the bright extended H II region S284 ($l, b \sim 212.^{\circ}0, -1.^{\circ}6$). Bonsignori-Facondi & Tomasi (1979) have investigated this source and its surroundings and decomposed the central H II region from a non-thermal component with a diameter of 67′.5. The spectral index for this non-thermal component, G211.7−1.1, is about $\alpha = 0.5$, typical for that of shell-type SNRs. Its apparent association with S284 gives a distance of about 2.4 kpc corresponding to a size of 46 pc.

The Effelsberg 863 MHz map (Fig. 8) shows the complex surroundings of S284, although the present angular resolution does not allow the study of details. However, we note that to the east of S284 a faint, but distinct emission plateau,

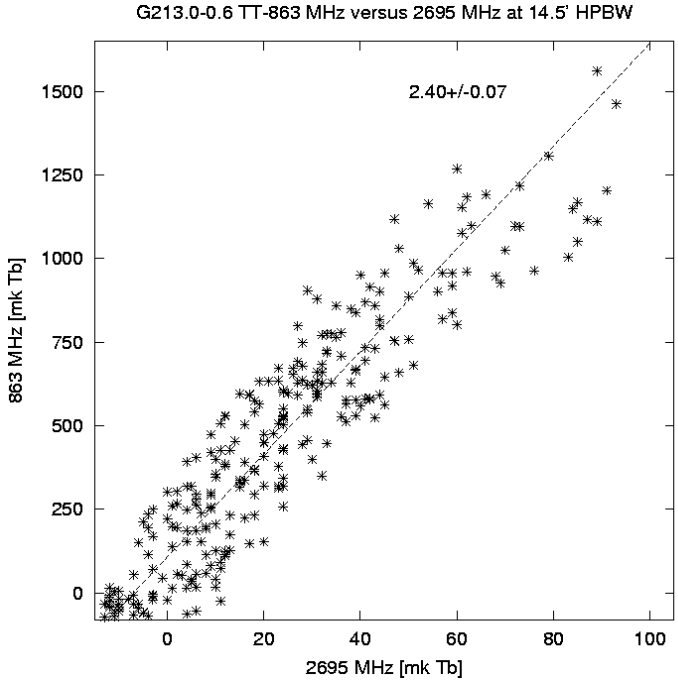


**Fig. 9.** Temperature-versus-temperature plot of G213.0−0.6 of a 30′ wide longitude strip at $b = -10'$ at 863 MHz and 2695 MHz. The strip is free from compact sources. The fit gives a temperature spectral index of 2.40 ± 0.15 ($\alpha = 0.40 \pm 0.15$).

G213.0−0.6, with an extent of about 160′×140′, is located. The morphology suggests that the partial shell-like emission near S284 is part of G213.0−0.6, which gets enhanced near S284. This may indicate some interaction. Although G213.0−0.6 is clearly visible in the Effelsberg surveys of the Galactic plane at 21 cm and 11 cm wavelength (Reich et al. 1997; Fürst et al. 1990) the spectral index and therefore its nature is difficult to determine precisely. We have in addition checked the IRAS 100 $\mu$m and 60 $\mu$m emission of this region and found extended emission north and south of S284, which partly overlaps with G213.0−0.6. The morphology indicates no association. From a differential spectral-index plot (TT-plot) between the 863 MHz data and the convolved 2.695 GHz data from the Effelsberg survey (Fig. 9) we derive a spectral index of $\alpha = 0.40 \pm 0.15$. This spectral index and missing associated dust emission makes a non-thermal origin of G213.0−0.6 likely.

The large size, its location in the Galactic plane and the partial shell-like structure close to S284 suggests a SNR identification of G213.0−0.6. A sign for an old evolved SNR is a low surface brightness and a large size. If G213.0−0.6 is in fact interacting with S284, as suggested by its morphology, its distance of 2.4 kpc can be adopted. This makes G213.0−0.6 about 110 pc × 98 pc in size and thus one of the largest SNRs known. After subtraction of all visible compact sources ( as marked in Fig. 8) a flux density of about 22.0 ± 3.7 Jy was obtained at 863 MHz. 18.0 ± 3.5 Jy were measured from the convolved Effelsberg survey map at 1.4 GHz in the same way. This flux integration confirms a spectral index of about $\alpha \sim 0.40$. We calculate a surface brightness of $1.4 \times 10^{-22}$ W m$^{-2}$ Hz$^{-1}$ sr$^{-1}$ at 1 GHz, which is one of the lowest measured surface brightness of Galactic SNRs.

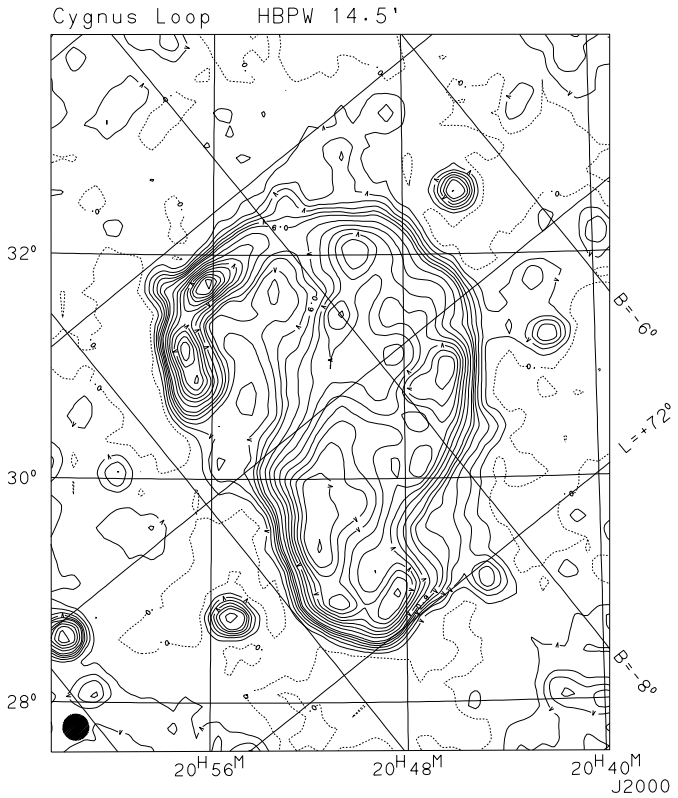


**Fig. 10.** Contour plot of the Cygnus Loop as observed at 863 MHz. Contours run in steps of 150 mJy/b.a. up to 900 mJy/b.a. and further in steps of 300 mJy/b.a.

### 3.7. G74.0−8.5 (Cygnus Loop)

The Cygnus Loop is a nearby well-studied large-diameter radio source located outside the Galactic plane with little confusing emission in its vicinity. Observations of the Cygnus Loop were already made in all wavelength ranges. It was often referred to as a proto-type for shell-type SNRs of medium age, although the source shape deviates significantly from a spherical shell. The Cygnus Loop (Fig. 10) was recently suggested by Uyanıker et al. (2002) to consist of two interacting SNRs: G74.3−8.4 and G72.9−9.0 with similar spectra. The angular resolution of 14′.5 at 863 MHz does not allow to distinguishing of both SNRs very well in their region of overlap. The 863 MHz map was already included in a spectral index study using Effelsberg maps partly complemented by DRAO data in the frequency range between 408 MHz and 2675 MHz. The integrated 863 MHz flux density of the Cygnus Loop of 184 ± 18 Jy fits quite well to the recent $\alpha = 0.42 \pm 0.06$ spectrum derived by Uyanıker et al. (2003) between 408 MHz and 2675 MHz, but is also consistent with the $\alpha = 0.49$ spectrum fitted by Trushkin (2002) for a frequency range from 22 MHz to 5 GHz. There is no indication of a spectral bend in its integrated spectrum, nor large spectral index variations across the SNR as reported before. The derived 863 MHz flux density is significantly more accurate than previous estimates in this frequency range as listed in Table 1 by Uyanıker et al. (2003).

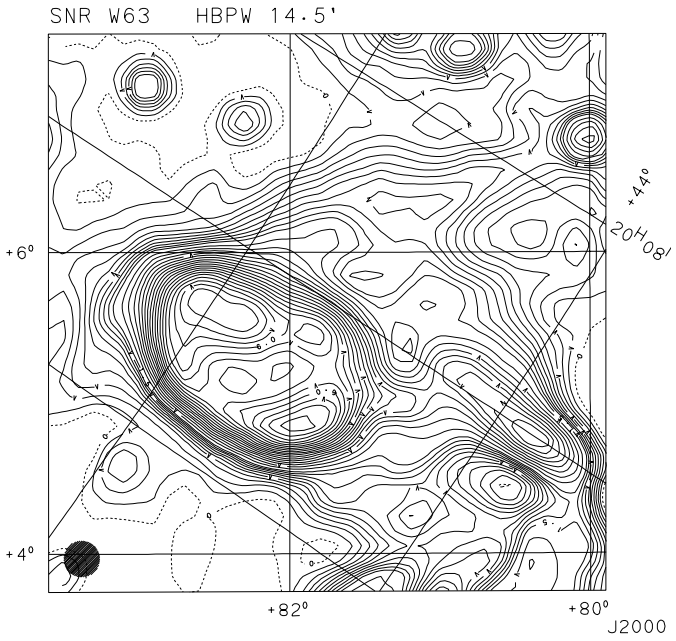


**Fig. 11.** Contour plot of W63 as observed at 865 MHz. Contours run in steps of 150 mJy/b.a. The contour at 1.5 Jy/b.a. and 6.0 Jy/b.a. are labelled.

### 3.8. G82.5+5.3 (W63)

The SNR W63 is located north of the Cygnus-X emission complex, where a superposition of emission structures from the local spiral arm along the line of sight is seen. Despite its high Galactic latitude of 5°.3 the surrounding structures of W63 are quite complex as visible in Fig. 11. We made an attempt to remove the underlying large-scale emission by applying the "background filtering" method by Sofue & Reich (1979). Using a 90′ filtering beam to separate the large-scale background we got an integrated flux density for W63 of 82.5±5.5 Jy. From the unfiltered map the flux density of W63 is about 11 Jy higher. In any case our flux density is significantly below that expected from the spectrum based on previous flux-density values. Higgs et al. (1991) have studied the area of W63 with the DRAO interferometer at 408 MHz and discussed the spectrum of W63 using available data from the literature. They found it difficult to clearly define a spectral index and quote values between $\alpha = 0.49$ and $\alpha = 0.62$. The fitted spectra predict about 140 Jy at 865 MHz, while our measured flux density is just about 60% of that value. Trushkin's fit (2002) with $\alpha = 0.5$ at 400 MHz and $\alpha = 0.53$ at 4 GHz predicts 144 Jy, while Kovalenko et al. (1994b) fitted $\alpha = 0.63 \pm 0.15$ and predict 120 Jy at 865 MHz.

We performed a tempertature-versus-temperature (TT) plot of the 865 MHz data and the 1.4 GHz data of W63 as shown in Fig. 12. The 1.4 GHz data were extracted from a map of Uyanıker et al. (1999). The fitted slope gives a spectral index of $\alpha = 0.37 \pm 0.09$. This is a slightly smaller value when compared to previous estimates, but the TT-plot method is rather insensitive to the influence of background emission. It is obvious that in the case of W63 most flux density measurements

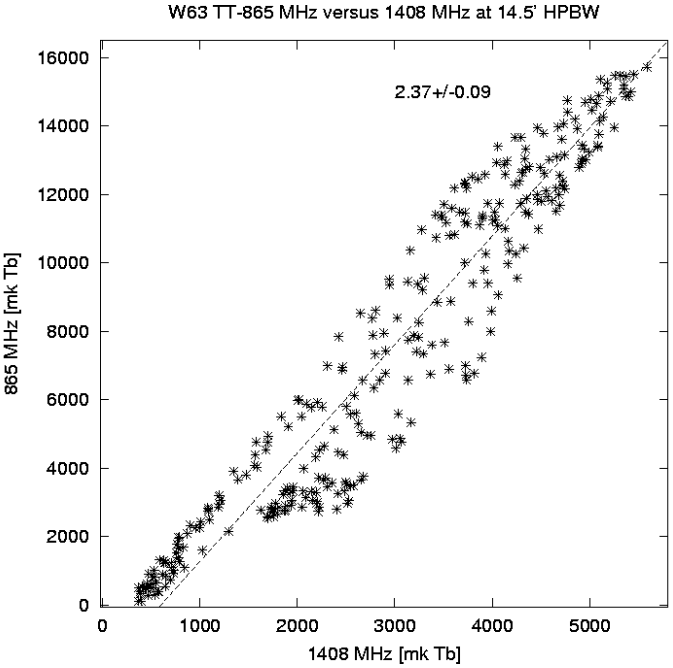


**Fig. 12.** Temperature-versus-temperature plot of W63 observed at 865 MHz and 1.4 GHz. The fit gives a temperature spectral index of $2.37 \pm 0.09$ corresponding to $\alpha = 0.37 \pm 0.09$.

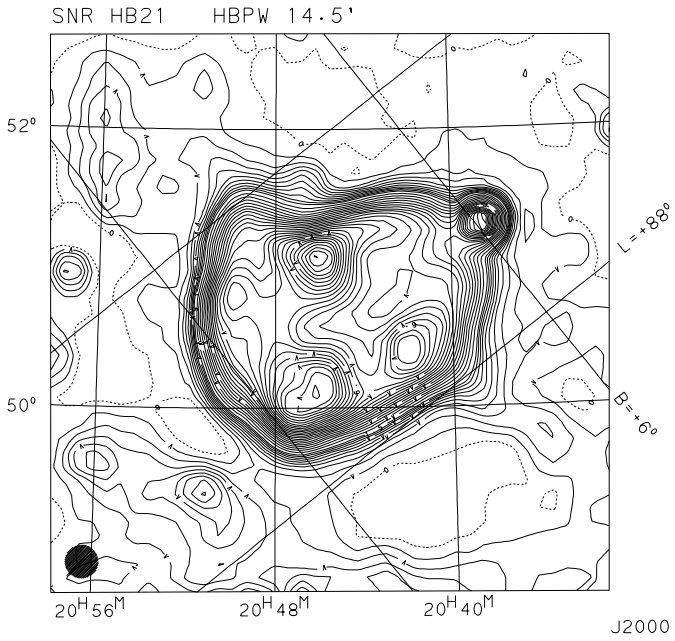


**Fig. 13.** Contour plot of HB21 as observed at 865 MHz. Contours run in steps of 150 mJy/b.a. up to 1.5 Jy/b.a. and in steps of 300 mJy/b.a. above.

made with a large beam size are too high, likely caused by insufficient separation of unrelated surrounding emission.

### *3.9. G89.0+4.7 (HB21)*

HB21 is a large diameter (1.°5×2°), strong radio source and was already detected in the early days of radio astronomy by Brown & Hazard (1953) at 159 MHz. HB21 is an evolved SNR with an unusual complex morphology and was observed at many frequencies. Tatematsu et al. (1990) made a detailed study of molecular material in interaction with the SNR. They derived a distance of $800 \pm 70$ pc for HB21. The radio spectrum of HB21 can be fitted by a single power law for frequencies above about 30 MHz. At frequencies below 30 MHz there is some indication of thermal absorption. Willis (1973) gives a spectral index of $\alpha = 0.40 \pm 0.03$, Trushkin (2002) fitted $\alpha = 0.38$, Kovalenko et al. (1994b) list $\alpha = 0.39 \pm 0.10$ and Zhang et al. (1996) report $\alpha = 0.41 \pm 0.02$. All these fits are similar. The 865 MHz image is shown in Fig. 13. The strong compact extragalactic radio source, 3C 418, is located at the north-western edge of HB21. It has a flux density of 5.4 Jy. Excluding 3C 418 we calculate an integrated flux density of $228 \pm 5$ Jy. This flux density agrees quite well with those predicted from the spectral fits made by Trushkin (2002), Kovalenko et al. (1994b) and Zhang et al. (1996) of 234 Jy, 233 Jy and 227 Jy, respectively. HB21 is located in a region with low Galactic emission in its surroundings so that flux determinations even with large beam sizes are quite reliable.

## 4. Concluding remarks

We have presented maps for a number of large-diameter SNRs at 35 cm wavelength from observations with the Effelsberg 100-m telescope. For sources with confusing emission in their surroundings we found flux densities well below those given in the literature, e.g. HB9, W63. Previous single-dish observations were made with lower angular resolution and sensitivity. Since the SNRs studied in this paper are strong radio sources, the discrepancy reflects not sensitivity differences but limitations when defining an adequate zero-level for measuring their integrated flux density with a large beam size. For a number of SNRs (e.g. the Cygnus Loop, HB21, S147) our flux densities agree with previous data although our errors are significantly smaller. For sources like W63 or HB3, having very strong Galactic emission in their vicinity, the flux densities measured with a 14.′5 beam might still be affected.

We tentatively identify a new large-diameter SNR G213.0−0.6 of very low surface brightness.

*Acknowledgements.* X.Z. acknowledges support from the MPG-CAS exchange program. We like to thank O. Lochner and his group for technical support. B. Uyanıker and P. Reich made helpful comments on the manuscript. We are grateful to the referee, Dr. J. Dickel, for his constructive comments.

## References

Anderson, S. B., Cadwell, B. J., Jacoby, B. A., et al. 1996, ApJ, 468, L55
Angerhofer, P. E., & Kundu, M. R. 1981, AJ, 86, 1003
Asaoka, I., & Aschenbach, B. 1994, A&A, 284, 573
Baars, J. W. M., Genzel, R., Pauliny-Toth, I. I. K., & Witzel, A. 1989, A&A, 61, 99
Berkhuijsen, E. M. 1972, A&AS, 5, 263

Bonsignori-Facondi, S., & Tomasi, P. 1979, A&A, 77, 91
Braun, R., & Strom, R. 1986, A&A, 164, 193
Brown, R. H., & Hazard, C. 1953, MNRAS, 113, 123
Emerson, D. T., & Gräve, R. 1988, A&A, 190, 353
Esposito, J. A., Hunter, S. D., Kanbach, G., & Sreekumar, P. 1996, ApJ, 461, 820
Fesen, R. A., Downes, R. A., Wallace, D., & Normandeau, M. 1995, AJ, 110, 2876
Fürst, E., Reich, W., Beck, R., Hirth, W., & Angerhofer, P. E. 1982, A&A, 115, 428
Fürst, E., Reich, W., & Steube, R. 1984, A&A, 133, 11
Fürst, E., & Reich, W. 1986, A&A, 163, 185
Fürst, E., Reich, W., Reich, P., & Reif, K. 1990, A&AS, 85, 691
Geldzahler, B. J., & Shaffer, D. B. 1981, ApJ, 248, L32
Geldzahler, B. J., & Shaffer, D. B. 1982, ApJ, 260, L69
Green, D. 1986, MNRAS, 221, 473
Harris, D. E. 1962, ApJ, 135, 661
Higgs, L. A., Landecker, T. L., Israel, F. P., & Bally, J. 1991, J. Roy. Astron. Soc. Can., 85, 25
Joncas, G., Roger, R. S., & Dewdney, P. E. 1989, A&A, 219, 303
Kim, K. 1988, J. Korean Astron. Soc., 21, 133
Kovalenko, A. V., Pynzar, A. V., & Udal'tsov, V. A. 1994a, AR, 38, 78
Kovalenko, A. V., Pynzar, A. V., & Udal'tsov, V. A. 1994b, AR, 38, 95
Kühr, H., Witzel, A., Pauliny-Toth, I. I. K., & Nauber, U. 1981, A&AS, 45, 367
Landecker, T. L., Vaneldik, J. F., Dewdney, P. E., Routledge, D. 1987, AJ, 94, 111
Leahy, D. A., Zhang, X., Wu, X., & Lin, J. 1998, A&A, 339, 601
Lochner, O., & Fürst, E. 1997, Testbericht UHF-Empfänger, 12.1997, MPIfR, Bonn
Lochner, O., & Fürst, E. 1998, Testbericht UHF-Empfänger, 10.1998, MPIfR, Bonn
Olbert, C. M., Clearfield, C. R., Williams, N. E., Keohane, J. W., & Frail, D. A. 2001, ApJ, 554, L205
Ott, M., Witzel, A., Quirrenbach, A., et al. 1994, A&A, 284, 331
Reich, P., Reich, W., & Fürst, E. 1997, A&AS, 126, 413
Romani, R. W., & Ng, C.-Y. 2003, ApJ, 585, L41
Sofue, Y., & Reich, W. 1979, A&AS, 38, 251
Sofue, Y., Fürst, E., & Hirth, W. 1980, PASJ, 31, 1
Spinrad, H., Stauffer, J., & Harlan, E. 1979, PASP, 91, 619
Sturner, S. J., & Dermer, C. D. 1995, A&A, 293, L17
Tatematsu, K., Fukui, Y., Landecker, T. L., & Roger, R. S. 1990, A&A, 237, 189
Trushkin, S. A. 2002, `http://cats.sao.ru`
Uyanıker, B., Fürst, E., Reich, W., Reich, P., & Wielebinski, R. 1999, A&AS, 138, 31
Uyanıker, B., Reich, W., Yar, A., Kothes, R., & Fürst, E. 2002, A&A, 389, L61
Uyanıker, B., Reich, W., Yar, A., & Fürst, E. 2003, A&A, submitted
Wang, Z., & Scoville, N. Z. 1992, ApJ, 386, 158
Westerhout, G. 1958, Bull. Astron. Inst. Neth., 14, 215
Willis, A. G. 1973, A&A, 26, 237
Zhang, X., Zhu, J., Higgs, L., & Landecker, T. L. 1996, J. Korean Astron. Soc., 29, 199